H2/Hinf robust lateral control of an off-road two-steering-axle vehicle on slippery sloping soils

Romain Legrand, Fabien Claveau, Philippe Chevrel, Benjamin Rancinangue, Anthony Dollet

H_2 / H_∞ robust lateral control of an off-road two-steering-axle vehicle on slippery sloping soils ⋆

Romain LEGRAND [*,**] **Fabien CLAVEAU** [*] **Fabien CLAVEAU** [*]
Benjamin RANCINANGUE [**] **Anthony DOLLET** [**]

[*] *IMT Atlantique, UBL, and also the LS2N Laboratory, UMR CNRS 6004, 44000 Nantes, France (email : firstname.lastname@imt-atlantique.fr)*
[**] *Secom Engineering, 44100 Nantes, France (email : rlegrand@secom.fr, brancinangue@secom.fr, adollet@secom.fr)*

Abstract: This paper presents an efficient design for a lateral control synthesis of an off-road vehicle. The considered vehicles have two steering axles and are intended to move on a slippery soil with important lateral and longitudinal slopes. The proposed design relies on an extended bicycle model that accounts for the slopes. The lateral control is designed based on a feedforward/feedback architecture. The feedforward takes advantage of the knowledge of the path characteristics (curvature and slopes), and the feedback ensures robust reference-trajectory tracking. Through an H_2 / H_∞ multi-objective synthesis, the robustness of the lateral controller is ensured with regard to the model uncertainties, path, and soil features. This is important because off-road vehicles' dynamics are by nature highly variable. To cope with the difficulty caused by uncertain knowledge of key parameters, the proposed robust approach is a practical compromise that maximizes performance under constraints of robustness. The results obtained on a realistic non-linear simulator support this assertion.

Keywords: Unmanned autonomous vehicles, Autonomous vehicles, Robust control, H infinity control, Motion control

1. INTRODUCTION

In recent years, robots have been used in many fields to execute tough and repetitive tasks and relieve burden on humans. Agriculture is one of the areas where this trend is most obvious : the agricultural robots market is projected to grow from USD 4.6 billion in 2020 to USD 20.3 billion by 2025, equating to annual growth of 34.5%, see Markets and Markets (2020). Path-following machines are a prominent market in the broad field of precision agriculture; they can be indoor devices (e.g., feeding robots) or outdoor vehicles such as harvesters or sprayers. The automation of trajectory tracking for the latter ones rose rapidly after the high GPS coverage in the last decade became more reliable and more accessible, see Bury et al. (2019). However, path following is challenged by slippery sloping soils, which tremendously affect a vehicle's dynamics.

On-road vehicles have to account for high speeds (mainly implemented using dynamical models), as in Mourad et al. (2014), Attia et al. (2012) or Rajamani (2012), whereas off-road vehicle research has been traditionally conducted using kinematic models, see Lenain et al. (2009) and Fernandez et al. (2019). However, a convergence in the research field has occurred in recent years in favor of dynamical modeling, see Derametz (2018), despite the numerous constraints that are ignored in on-road path following modeling, such as the lack of grip or the presence of slopes. This convergence has led to homogenization in the tools used in different contexts. The H_2 / H_∞ control design used in this paper has been previously used in the on-road context to ensure robustness of the regulator, as in Mustaki et al. (2019).

The overall goal of the research presented here was to develop an embedded control system regulating both lateral and longitudinal dynamics of an off-road vehicle that is subject to high slips due to the environment. For this purpose, we chose to use two steering axles and the torques on each wheel for achieving the actuating actions. It is quite common to encounter vehicles equipped with two steering axles in the agricultural context where complex maneuvers are needed in restricted areas, see Fnadi et al. (2019). This configuration has proven its capabilities in recently published studies as in Derametz et al. (2017). This paper focuses on lateral control using an extended bicycle model as a control-synthesis model. This allows the modeling of slips on both rear and front steering axles in numerous situations, including slopes. It is well known that the lateral bicycle model implies some strong assumptions, such as constant longitudinal velocity, the omission of the height of the center of gravity, and the absence of dynamics between wheels within the same axle. However, in this work, it is demonstrated that this model is still useful even in the complex off-road environment.

The extended bicycle model is used to design a controller with two degrees of freedom. The feedforward term benefits from the knowledge of the path characteristics (curvature and slope), and the feedback term ensures robust tracking by removing the residual deviations. The precise management of the performance robustness compromise ensured by the H_2 / H_∞ control synthesis (see Apkarian et al. (2014)) has

⋆ This work was supported by the French government through ANRT (Association Nationale Recherche Technologie) fundings.

proven its efficiency, especially in the automotive field as in Mustaki et al. (2018). In Mustaki et al. (2018), a multi-model approach was used to capture various dynamics due to some parameters' uncertainties.

This paper is organized as follows. In Section 2, the extended bicycle model that considers slopes is introduced. Section 3 defines the architecture of the multivariable lateral controller. The definition of the uncertainties considered in this paper is found in Section 4. Section 5 describes the two stages of robust control synthesis including the optimization problem formulation. Finally, the results from a realistic simulator are presented in Section 6.

CG	Center of gravity
F,R	Index for the front / rear axle
m	Vehicle total mass [kg]
I_z	Vehicle inertia w.r.t the vertical axis [kg.m^2]
L	Wheelbase of the vehicle [m]
t	Track width of the vehicle [m]
L_F,L_R	Distance of the CG to the front/rear axle [m]
t_L,t_R	Distance of the CG to the left /right track [m]
h	Height of the CG [m]
C_i	Cornering stiffness of the wheel i [N]
c_i	Static cornering stiffness
$F_{j,a}$	Force w.r.t axis a on axle j [N]
$F'_{z,a}$	Normal force on axle j w.r.t the z axis of the global frame [N]
$p_{\min}$, $p_{\max}$	Minimal and maximal value of the parameter p
$\overline{p}$	Nominal value of the parameter p
$\mathscr{M}$	Set of synthesis linear models considered to define the uncertain vehicle model, comprised of N instances
$\mathscr{M}_i$	Instance of $\mathscr{M}$
v_x,v_y	Longitudinal / Lateral vehicle speed, at the CG in the vehicle's frame [m.s^{-1}]
a_x,a_y	Longitudinal / Lateral vehicle acceleration [m.s^{-2}]
$F_{y,i}$,$F_{z,i}$	Lateral / Vertical forces applied on wheel i [N]
$\dot{\psi}$	Yaw speed of the vehicle [rad.s^{-1}]
δ_i	Steering angle of wheel i [rad]
δ_F,δ_R	Mean Ackermann steering angle of the front /rear axle [rad]
δ	$= (\delta_F \quad \delta_R)^T$
δ_{FF}	Feedforward values of the steering angles [rad]
δ	$= (\delta_F \quad \delta_R)^T$
ρ	Curvature of the reference trajectory [m^{-1}]
φ, θ	Lateral / Longitudinal slope angle [rad]
ρ_{mes}, φ_{mes}	Measured curvature / Lateral slope angle [m^{-1}]/[rad]
α	Local value on the soil's slope [rad]
μ	Coefficient of adhesion
g	Acceleration of gravity [m.s^{-2}]
y	Lateral deviation w.r.t. the reference trajectory [m]
$\tilde{\psi}$	Angular deviation w.r.t. the reference trajectory [rad]
x	$= (\tilde{\psi} \quad \dot{\psi} \quad y \quad \dot{y})^T$, state vector
x_{FF}	Feedforward state vector, considered as a reference
x_s	Difference between x and x_{FF}
z	$= (\tilde{\psi} \quad y)^T$, controlled outputs
s	Laplace operator
$T_{i\to o}^{\mathscr{M}_k}$	Transfer function between input i and output o for for k^{th} instance of $\mathscr{M}$

Table 1. List of symbols and abbreviations

2. TWO-STEERING-AXLE BICYCLE MODEL CONSIDERING SLOPES

The model introduced in this section aims to support the design of the lateral controller. The level of complexity must be parametrized carefully to be able to consider a two-steering-axle vehicle in slopes and to be simple enough to be handled properly. An extended bicycle model was therefore chosen to take into account the large variability of the vehicle and its environment.

The overall goal is to define a family of linear models with the same structure but different sets of parameters to encompass the realistic range of variations of key parameters (see Subsection 4.3). It is necessary to identify and express as many independent variables as possible. For example, the cornering stiffness of the pneumatic (function of the normal forces on the wheel) is highly related to the total mass of the vehicle and the location of the CG, among other factors. The situation in Fig. 1 can be represented by (1) using the fundamental principle of the dynamics on the vertical axis and its rotational equivalent on the lateral axis (see Tab. 1 for the definition of the parameters) :

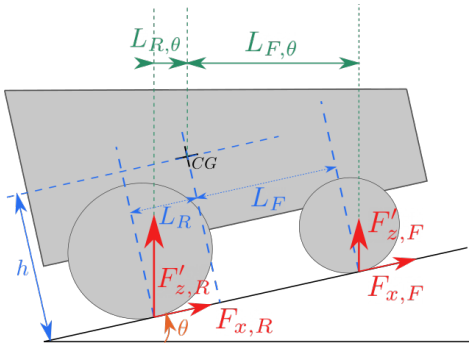

Fig. 1. Load distribution on a longitudinal slope

$$\begin{cases} F_{z,F} + F_{z,R} = mg\cos(\alpha) \\ I_y\ddot{\theta} = h\overbrace{(F_{x,F}+F_{x,R})}^{ma_x} + \overbrace{(L_F + h\tan(\theta))}^{L_{F,\theta}} F_{z,F} - \overbrace{(L_R - h\tan(\theta))}^{L_{R,\theta}} F_{z,R} \end{cases} \tag{1}$$

You can note according to Fig. 1 and (1) that $F'_{z,FR}$ and $F'_{z,RR}$ (along the global frame's z axis) are considered instead of $F_{z,FR}$ and $F_{z,RR}$ (along the vehicle's frame's z axis). It allows the estimation of the actual loads supported by the wheels and thus the actual cornering's stiffnesses. These coefficients' formulas are described in (2) using (1), ignoring a_x and $\ddot{\theta}$ (constant longitudinal speed and slope assumption), and assuming that the cornering stiffness C_i is proportional to μ, $F_{z,i}$ and c_i as in Rill (2013).

$$\begin{cases} C_F = c_F \mu F_{z,F} \\ C_R = c_R \mu F_{z,R} \end{cases} \quad \text{with} \quad \begin{cases} F_{z,F} = mg\cos(\alpha)\dfrac{L_R - h\tan(\theta)}{L} \\ F_{z,R} = mg\cos(\alpha)\dfrac{L_F + h\tan(\theta)}{L} \end{cases} \tag{2}$$

It is possible to express the lateral forces applied on each wheel of the bicycle model. Although advanced models can compute these forces (see Bakker et al. (1987), Hirschberg et al. (2003)), a linearized version may be sufficient to provide behavioral trends. Forces are considered proportional to the slip angle. The $\cos(\theta)\cos(\varphi)$ term in L'_F and L'_R definitions comes from the vehicle's frame in Fig. 2 while v_{ya} is the lateral speed at the wheel axis a.

$$\begin{aligned} F_{y,i} &= C_i\beta_i \\ &= C_i\left(\delta_i - \frac{v_{yi}}{v_x}\right) \end{aligned} \quad \text{with} \quad \begin{cases} v_{yF} = v_y + L_F\cos(\theta)\cos(\varphi)\dot{\psi} \\ \qquad = v_y + L'_F\dot{\psi} \\ v_{yR} = v_y - L_R\cos(\theta)\cos(\varphi)\dot{\psi} \\ \qquad = v_y - L'_R\dot{\psi} \end{cases} \tag{3}$$

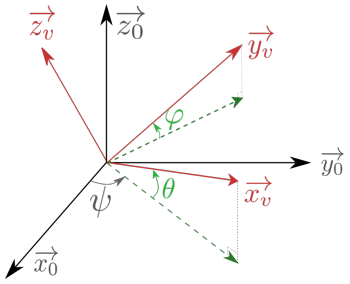

Fig. 2. Vehicle frame's definition

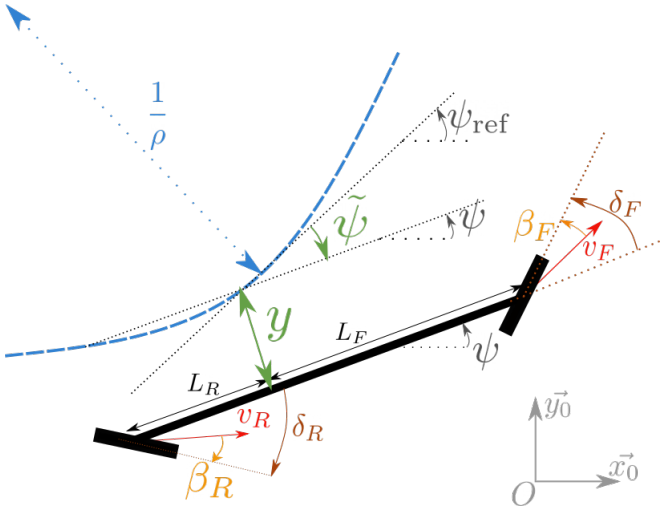

Fig. 3. Bicycle model

The classical kinematic evolution of the deviations (4) can be found in Mustaki (2019) (see also Fig. 3) :

$$\begin{cases} \dot{y} = v_y + v_x\tilde{\psi} \\ \dot{\tilde{\psi}} = \dot{\psi} - v_x\rho \end{cases} \tag{4}$$

The state equations are finally obtained using (3), (4), and the fundamental principles of the dynamics of rotation and translation .

$$\begin{aligned} \ddot{y} &= \frac{d}{dt}\left(v_y + v_x\tilde{\psi}\right) = \dot{v}_y + v_x\left(\dot{\psi} - v_x\rho\right) = a_y - v_x^2\rho \\ &= \frac{F_{y,F} + F_{y,R}}{m} - g\sin(\varphi) - v_x^2\rho \\ \ddot{y} &= -\frac{C_F + C_R}{m v_x}\dot{y} + \frac{C_F + C_R}{m}\tilde{\psi} + \frac{L'_R C_R - L'_F C_F}{m v_x}\dot{\psi} + \frac{C_F\delta_F + C_R\delta_R}{m} \\ &\quad - g\sin(\varphi) - v_x^2\rho \end{aligned} \tag{5}$$

$$\begin{aligned} \ddot{\psi} &= \frac{L'_F(F_{y,FL} + F_{y,FR}) - L'_R(F_{y,RL} + F_{y,RR})}{I_z} \\ &= \frac{L'_R C_R - L'_F C_F}{I_z v_x}\dot{y} + \frac{L'_F C_F - L'_R C_R}{I_z}\tilde{\psi} \\ &\quad - \frac{L'^2_F C_F + L'^2_R C_R}{v_x I_z}\dot{\psi} + \frac{L'_F C_F\delta_F - L'_R C_R\delta_R}{I_z} \end{aligned} \tag{6}$$

By defining the state vector $x = \left(\tilde{\psi}\ \dot{\psi}\ y\ \dot{y}\right)^T$, the command vector $\delta = \left(\delta_F\ \delta_R\right)^T$ and the exogenous inputs $d = \left(\rho\ \sin(\varphi)\right)^T$, the linear lateral synthesis model of the vehicle $\dot{x} = Ax + B\delta + Gd$ can be obtained using (4), (5), and (6). It is possible to replace C_i by its less common expression in (2).

$$A = \begin{pmatrix} 0 & 1 & 0 & 0 \\ \frac{L'_F C_F - L'_R C_R}{I_z} & -\frac{L'^2_F C_F + L'^2_R C_R}{I_z v_x} & 0 & \frac{L'_R C_R - L'_F C_F}{I_z v_x} \\ 0 & 0 & 0 & 1 \\ \frac{C_R + C_F}{m} & \frac{L'_R C_R - L'_F C_F}{m v_x} & 0 & -\frac{C_R + C_F}{m v_x} \end{pmatrix} \tag{7}$$

$$G = \begin{pmatrix} -v_x & 0 \\ 0 & 0 \\ 0 & 0 \\ -v_x^2 & -g \end{pmatrix}, \quad B = \begin{pmatrix} 0 & 0 \\ \frac{L'_F C_F}{I_z} & -\frac{L'_R C_R}{I_z} \\ 0 & 0 \\ \frac{C_F}{m} & \frac{C_R}{m} \end{pmatrix}$$

Several parameters in (7), such as θ, φ, α, c_i, and μ, are not easy to measure or estimate, and they can vary dramatically during agricultural tasks. That is why it is crucial to create a lateral regulator that is robust to this kind of uncertainties. Note that both slopes are included in the definition of this model (θ in (2) and φ in (5)). The load transfers are thus satisfactorily considered in (7).

3. ARCHITECTURE OF THE REGULATION SYSTEM

The overall architecture of the control law is shown in Fig. 4. It is based on two matrix gains that are designed sequentially. First, the feedforward term δ_{FF} and the reference state x_{FF} are calculated from the measures of the curvature of the reference path and the lateral slope angle (see Subsection 5.1 for the design methodology). Second, having access to both steering actuators (δ_F and δ_R) makes it possible to regulate both the lateral deviation y and the angular deviation $\tilde{\psi}$, see Rajamani (2012). To do so, a state augmentation is implemented in the feedback part incorporating the integrals $\int y$ and $\int\tilde{\psi}$. This augmented state vector X_s, incorporating both the reference state and the measures, is used to calculate the feedback command δ_K. It is based on classical considerations from Wonham's internal model by using the matrix K (8), as δ_K=KX_s. It constitutes the state feedback part of the controller : a multivariable PI controller, see Kwakernaak and Sivan (1969).

$$K = \begin{pmatrix} k_{\int\tilde{\psi},F} & k_{\tilde{\psi},F} & k_{\dot{\psi},F} & k_{\int y,F} & k_{y,F} & k_{\dot{y},F} \\ k_{\int\tilde{\psi},R} & k_{\tilde{\psi},R} & k_{\dot{\psi},R} & k_{\int y,R} & k_{y,R} & k_{\dot{y},R} \end{pmatrix} \tag{8}$$

Each gain in K is computed based on H_2/H_∞ multi-objective control synthesis. This methodology enables the definition of performance objectives on the regulated variables and supports robustness (see Section 5.2 for more information).

4. CONTROL DESIGN FRAMEWORK

4.1 Overview of the control design framework

The control framework is illustrated in Fig. 4. In the center, a set $\mathcal{M}$ of realistic linear models represents various possible

dynamics of the vehicle. The uncertain model leading to this multi-model formulation is depicted in the Subsection 4.3.

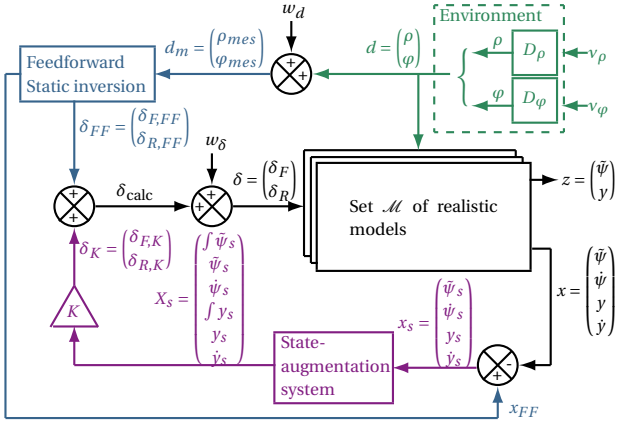

Fig. 4. Control design scheme. Feedforward and feedback control are in blue and purple respectively; generator models of exogenous signals are in green (path curvature and slope)

The controlled output grouped in vector z are the lateral deviation y and the angular deviation $\bar{\psi}$ (see Fig. 3). w_d and w_δ denote exogenous and input noises, respectively. The other inputs, ν_ρ and ν_φ, are irreducible signals providing the generator models of the two exogenous signals : the path curvature ρ and the slope angle φ.

4.2 Generator models

To provide some information about the dynamics of the environment's disturbances (ρ and φ), generator models are considered. The generator models provide some average information about the signals (see Chevrel (2013)) and are integrated in the formalization of the previously mentioned H_2/H_∞ objective control synthesis. The transfer functions D_ρ and D_φ (green part in Fig. 4) are the interface between $d = \begin{pmatrix}\rho & \varphi\end{pmatrix}^T$ and the irreducible signals ν_ρ, ν_φ. They reflect a scenario deviating temporarily from the nominal behavior (straight line and zero slopes). Precisely, starting from 0 (curvature and slopes and their derivatives), they can evolve jointly or separately until reaching a realistic extremum before returning to the nominal behavior. The respective maximum admissible values, $\frac{1}{8}m^{-1}$ and 21.8 deg (corresponding to a 40% slope) are high but achievable in vineyards. These information are taken into account to finally choose the third-order models in (9) inspired by the one proposed in Mustaki et al. (2018). Numerical values for parameters in (9) are found in section 6.1. They are coherent with respect to the realistic evolution of these signals.

$$\begin{cases} D_\rho(s) = \dfrac{\rho(s)}{\nu_\rho(s)} = \dfrac{\rho_{\max}}{(1+\tau_\rho s)\left(1+\dfrac{2\xi_\rho}{\omega_\rho}s+\dfrac{s^2}{\omega_\rho^2}\right)} \\ D_\varphi(s) = \dfrac{\varphi(s)}{\nu_\varphi(s)} = \dfrac{\varphi_{\max}}{(1+\tau_\varphi s)\left(1+\dfrac{2\xi_\varphi}{\omega_\varphi}s+\dfrac{s^2}{\omega_\varphi^2}\right)} \end{cases} \tag{9}$$

The impulse response of the generator models (Fig. 5) highlight the scenarios considered for control synthesis, with the curvature ρ and the lateral slope φ increasing in a short period of time before reverting to the nominal situation (straight line on flat ground). The embedded controller has access to the real measurements (or estimations) of the curvature and the slope. These generator models are thus only used to give a plausible evolution of φ and ρ with respect to random excitations ν_φ and ν_ρ while solving the optimization problem presented in Section 5.2 from the control design in Fig. 4 .

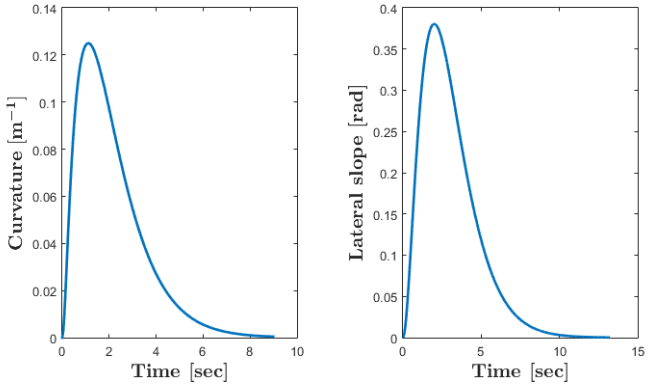

Fig. 5. Impulse responses of the curvature (left) and lateral slope (right) models

4.3 Definition of the uncertain synthesis model

In Tab. 2, the intervals of variation of the parameters are defined, which are deliberately wide (but realistic) in order to take into account the numerous configurations required by the vehicle when performing agricultural tasks. For example, the mass of the vehicle increases (respectively decreases) during harvesting (respectively spraying), which modifies the distribution of the masses (described by the L_F/L ratio parameter) at the same time.

Parameters	$p_{\min}$	$\overline{p}$	$p_{\max}$
μ	0.4	0.45	0.8
m [kg]	5000	6000	12000
$\frac{L_F}{L}$	0.2	0.43	0.8
t_L [m]	0.63	0.90	1.18
c_i	11.91	17.02	22.13
$\cos(\theta)\cos(\varphi)$	0.926	1	1

Table 2. Intervals of the varying parameters

The minimal value of $\cos(\theta)\cos(\varphi)$ is a physical limitation for a 40% slope ($\alpha_{\max} = 0.38$ rad or 21.8 deg), value encountered in the viticulture context. The uncertain value $h\tan(\theta)$ is needed to define C_i according to (2). Instead of adding another varying parameter, it is preferable to include this uncertainty in the parameter L_F, which is considered unknown in a broader extent. In addition, this wide uncertainty allows an implicit inclusion of suspensions that are ignored in the linear lateral model.

Using (2) for all combinations of the independent uncertain variables in Tab. 2 allows the evaluation of the realistic range of variation for the values of C_i. This methodology can be replicated for I_z and L'_i to exclude the unrealistic combinations of dynamical parameters. The realistic parameters' combinations obtained are represented in the spider web chart in Fig. 6 where colored polygons can be interpreted as instances of the vehicle synthesis model $\mathscr{M}$.

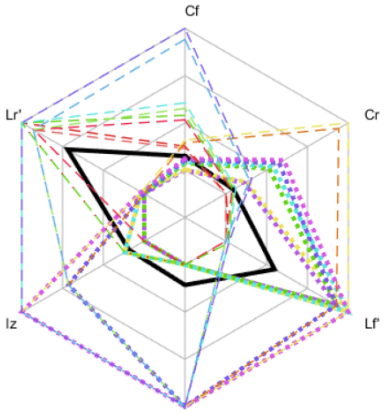

Fig. 6. Dispersion of the uncertain parameters. Each colored polygon defines a particular model by combining parameters' values within intervals described in Tab. 2

. The black polygon connect the nominal values of the parameters.

5. FEEDFORWARD AND FEEDBACK CONTROL DESIGN

5.1 Feedforward control design : static model inversion

One simple yet efficient solution for model based control is to proceed to a static inversion from the output references to determine the command, that is the steering angles δ_{FF} needed to follow the reference path. The curvature and the lateral slope angle constitute the inputs of the feedforward function, that helps calculate the reference state x_{FF} and the steering angles δ_{FF}. In this situation, the algebraic equation $0 = Ax_{FF} + B\delta_{FF} + Gd_m$ holds. By defining the reference state as $y_{FF} = \dot{y}_{FF} = \tilde{\psi}_{FF} = 0$ according to the control objectives, it is possible to invert the system to obtain x_{FF} and δ_{FF} in (10).

$$\begin{cases} 0 = Ax_{FF} + B\delta_{FF} + Gd_m \\ y_{FF} = \dot{y}_{FF} = \tilde{\psi}_{FF} = 0 \end{cases} \Longleftrightarrow \begin{cases} \delta_{FF} = F_\delta d_m \\ x_{FF} = F_x d_m \end{cases}$$

with

$$F_\delta = \begin{pmatrix} L'_F + \dfrac{L_R m v_x^2}{LC_F} & \dfrac{mgL_R}{LC_F} \\ -L'_R + \dfrac{L_F m v_x^2}{LC_R} & \dfrac{mgL_F}{LC_R} \end{pmatrix}, \quad F_x = \begin{pmatrix} 0 & 0 \\ v_x & 0 \\ 0 & 0 \\ 0 & 0 \end{pmatrix} \tag{10}$$

Contrarily to the other state variables, the value of $\dot{\psi}_{FF} = v_x\rho$ is not deduced from the control objectives but from the resolution of the algebraic equation $0 = Ax_{FF} + B\delta_{FF} + Gd_m$. In the following, the feedforward control synthesis is based on the nominal values of the vehicle parameters, while the feedback control synthesis takes into account uncertainties relying on the multi-model presented in 4.3.

5.2 Feedback control design : H_2/H_∞ optimization problem formulation

A H_2/H_∞ control problem is formulated to design the feedback matrix K (8). This solution must be robust enough to meet all the generic control specifications for all instances $\mathcal{M}_i$ of $\mathcal{M}$, defined in Subsection 4.3 based on the uncertain parameters in Tab. 2.

The objective function is defined to maximize path following performances regarding the curvature, which is the main objective of the lateral control system. The constraints are thoroughly elaborated to ensure the robustness and the stability of the controller. While the optimization criteria (C1) and (C2) concern performance despite lateral slope and measure errors, (C3) and (C4) ensure the control robustness and (C5) the closed loop dynamics. The robustness margins are formalized through an H_2 objective and H_2 or H_∞ hard constraints on closed loop transfers. These robustness margins constraints must be introduced to handle the nonlinearities that are neglected in (7). One can show that robustness is acquired regarding those nonlinearties by the small gain theorem (see Zames (1996)) and the circle criterion (see Arcak and Kokotović (2001)).

The optimization problem (OP), which purpose is to compute the feedback gains in K, is defined below (refer to Tab. 1 and Fig. 4 for notations). The parameters γ_j ($j \in \{\varphi, d, \text{mod}, \text{dyn}, \beta, \text{real}\}$) are tuning gains chosen according to the control specifications (see Section 6.1 for typical values)

$$\begin{aligned} &\text{minimize} && P_z = \max_{i\in[1,N]} \left\| T^{\mathcal{M}_i}_{v_\rho \to z} \right\|_2 \\ &\text{under constraints} \\ &\forall i \in [1,N] && (C1) : M_\varphi = \left\| T^{\mathcal{M}_i}_{v_\varphi \to z} \right\|_2 \leqslant \gamma_\varphi \\ & && (C2) : M_d = \left\| T^{\mathcal{M}_i}_{w_d \to z} \right\|_2 \leqslant \gamma_d \\ & && (C3) : M_{\text{mod}} = \left\| T^{\mathcal{M}_i}_{w_\delta \to \delta} \right\|^{-1}_\infty \geqslant \gamma_{\text{mod}} \\ & && (C4) : M_{\text{dyn}} = \left\| s T^{\mathcal{M}_i}_{w_\delta \to \delta} \right\|^{-1}_\infty \geqslant \gamma_{\text{dyn}} \\ & && (C5) : \text{Poles constraints} \begin{cases} \text{-damping ratio } \gamma_\beta \\ \text{-maximum real part } \gamma_{\text{real}} \end{cases} \end{aligned} \tag{OP}$$

The H_2 criterion P_z handles the tracking performance and penalizes the lateral (y) and angular ($\tilde{\psi}$) deviations with respect to the evolution of the curvature. (C1) (resp. (C2)) ensures low sensibilities of the deviations with respect to the evolution of the slopes of the ground (resp. to white noises on the measurements of slope and curvature). (C3) represents the input sensitivity constraint ensuring robustness regarding the actuators, in terms of modulus margin and circle criterion. (C4) is the high-frequency weighted complementary sensitivity constraint. It guarantees the robustness against high-frequency uncertainties and time delays. (C5) constrains the localization of the closed-loop poles by the parameters γ_{real} and γ_β (see Fig. 7).

Nonlinear and non-smooth optimization techniques were applied to solve the multi-criterion optimization problem (see (OP), Apkarian et al. (2014), Mustaki et al. (2018) and Walter and Noll (2015). Sub-gradients and a favorable initialization allow rapid convergence of the parameters of the target control architecture. Systune (MATLAB ®) was used to solve this problem (Sadabadi and Peaucelle (2016)) while considering the previously detailed constraints.

6. RESULTS

6.1 Gains design

The feedforward part was designed according to (10). Nominal values of the parameters are considered to be consistent with the tuning considered in the optimization of the

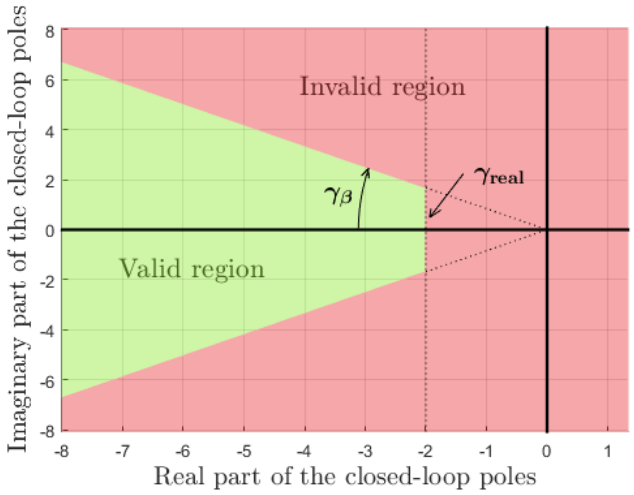

Fig. 7. Constrained location of the closed-loop poles

feedback gain. The optimization (OP) of the feedback gains completes the overall control architecture by taking into account the feedforward and the selection of the parameter set defined in Tab. 2 and Fig. 6. The longitudinal velocity of the vehicle is considered, being a measured time-varying parameter of the bicycle model. Adaptation to vehicle speed can be obtained using gain-scheduling, as in Apkarian et al. (2014) or Huang et al. (2014). The impact of the longitudinal velocity to the solution of (OP) and consequently to the performance-robustness trade-off may be assessed with reference in Tab. 3, in which robustness constraints are tuned as follows : $\gamma_\varphi = 1, \gamma_d = 2$, $\gamma_{\text{mod}} = 0.75$, $\gamma_{\text{dyn}} = 0.5$, $\gamma_\beta = 40°$ and $\gamma_{\text{real}} = -0.5$. These margins are tuned accordingly to classical specifications in terms of modulus margin as well as for the dynamic margin M_{dyn}. The latter makes it possible to robustify the control with respect to neglected high frequency dynamics or even delays (see Mustaki et al. (2018) and De Larminat (2007)). The generator models' parameters are the following : $\omega_\rho = \omega_\varphi = 1$, $\xi_\rho = 1.5$, $\xi_\varphi = 1$, $\tau_\rho = 0.1$ and $\tau_\varphi = 1$.

v_x [km/h]	3	4.5	6	7.5	10
P_z	0.0002	0.0005	0.0010	0.0016	0.0034
M_φ	0.0635	0.0914	0.1144	0.1439	0.2028
M_d	0.4025	0.6064	0.8142	1.0225	1.3724
M_{mod}	0.7505	0.7506	0.7503	0.7511	0.7529
M_{dyn}	0.5001	0.5003	0.5001	0.5005	0.5011

Table 3. Results of the optimization problem

It can be observed that the limiting constraints for this optimization problem are the ones linked to (C3) and (C4) robustness margins, which are close to specifications. Regarding the performance achieved despite the slope angles (C1) and measured noises (C2), they are more and more challenged while the longitudinal speed increases, to the point that they can't be strictly met at higher speeds ($\geqslant 15$ km/h) considering the chosen tuning of (OP).

6.2 Tests and simulator presentation

Simulator The 10 DOF simulator, running on MATLAB ®Simulink relies on a dynamical model and considers non-linear physical phenomena that are not described in the synthesis model such as the rolling resistance, the lateral and longitudinal slip forces on the 4 wheels with a pneumatic model tailored for agricultural purposes (see model on Hirschberg et al. (2003)), and the load transfers between all the wheels (as in Shuai et al. (2014)) depending on accelerations and slopes. The longitudinal and lateral dynamics are simulated without any decoupling assumption (Jazar (2009)). The steering actuators and all sensors (taking into account sampling frequencies, noises and offsets) are finely modeled, and no suspension is considered (vehicle with an infinitely high spring rate).

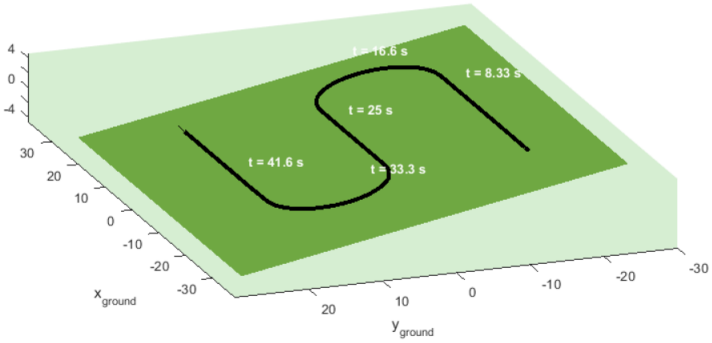

Fig. 8. Path of the simulation scenarios

Scenario on simulator The realistic scenario for the validation of this control architecture is presented in Fig. 8. On a constant slope of 10 degrees, the vehicle must do two 180° turns, each one associated with a curvature of $\frac{1}{8}\text{m}^{-1}$, at the constant speed of 10 km/h. One robust feedback controller is computed at this speed by solving (OP). To analyze its robustness, it was tested on five different configurations of the vehicle, all within $\mathcal{M}$ and representative of the wide scope of the uncertain models. Regarding the adherence, two configurations are defined by the product μc_i (a small value represents a small adherence between the wheels and the soil). As for the mass distribution, the simulations consider a vehicle capable of bearing an additional mass equal to its own. This extra mass, located at the rear part of the vehicle, changes the location of the CG (quantified by the ratio L_F/L) as well. The parameters of the nominal situation are shown in the middle column of Tab. 2, while the characteristics of the loaded and unladen vehicle are shown in Tab. 4. In the feedforward function (10), the values are set by the nominal situation. As a consequence, the parametrization of this function is flawed for the non-nominal configurations; thus, the global robustness of the control architecture is tested.

Parameters	Unladen	Loaded	Evolution
Total mass m	5000 kg	10000 kg	+100%
Ratio $\frac{L_F}{L}$	0.395	0.569	+44%

Table 4. Parameters of the vehicle in the simulations

6.3 Simulation results

Fig. 9 illustrates the lateral and angular deviations for the five configurations defined earlier. The performances for the nominal and unladen vehicle are particularly satisfactory (less than 5 cm and 2 deg), even in turns on low adherent

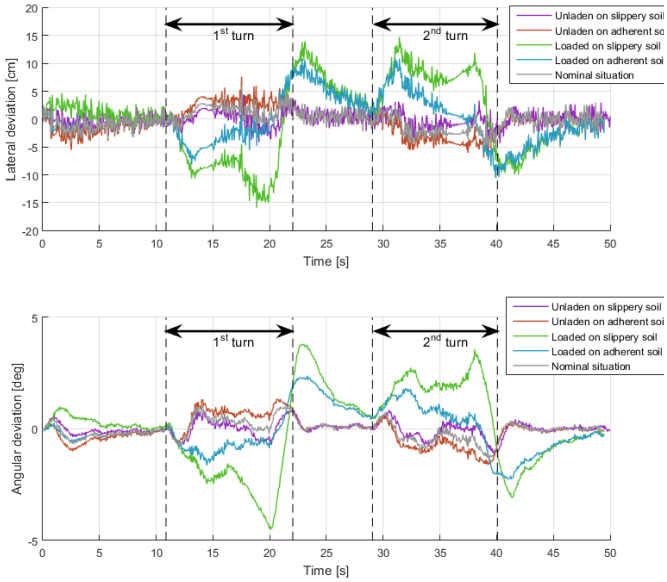

Fig. 9. Lateral and angular deviations

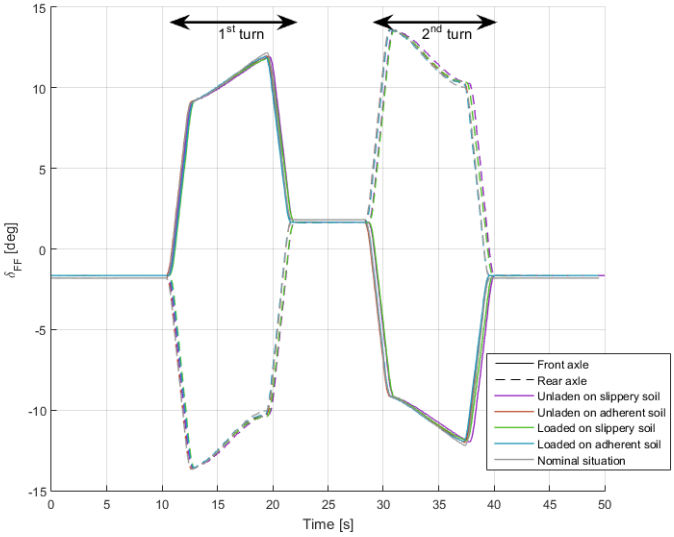

Fig. 10. Evolution of the front (continuous) and rear (dashed) feedforward term

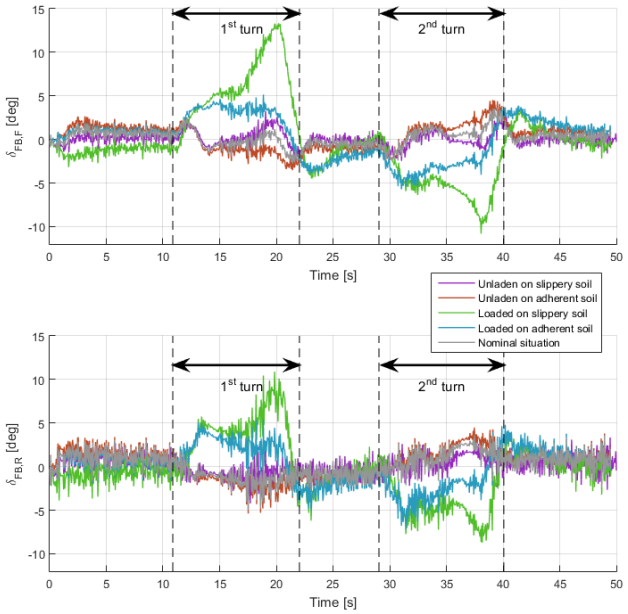

Fig. 11. Evolution of the front (top) and rear (bottom) feedback term

slopes. In the unladen configuration, the flawed parametrization of the feedforward function does not seem to affect the overall performance of the regulation.

As for the loaded vehicle, the results in straight lines are encouraging considering the firm and steady decrease of the deviations despite the important lateral slope angle. In turns, the deviations increase noticeably, even more in the case of slippery soil. Although more important, the deviations remain restrained and quite satisfactory in turns (15 cm and 5 deg). Notice that the configuration considering the loaded vehicle on adherent soil is the most distinct from the nominal situation, but it shows better results than the same configuration on a slippery soil because of the greater adherence.

The evolution of the feedforward terms for both axles in all scenarios is depicted in Fig. 10. They are all the same because of the common parametrization of the feedforward as mentioned earlier. In straight lines, the feedforward term considers the lateral slope in both axles ($\delta_{FF} \neq 0$), resulting in a crab steering mode. Moreover, the computed steering angles' values change while turning due to the evolution of the slope and curvature. All these observations show the strong capability of adaptation of the feedforward function to numerous situations.

Fig. 11 depicts the evolution of the feedback term for both axles and illustrates the quality of the feedforward function and the good synergy between both actions. The feedback terms remain quite close to zero for most of the situations except when the loaded vehicle is considered. In that case, the feedback contribution becomes stronger, especially in the bend, to assist the feedforward which seems to provide insufficient steering angles.

7. CONCLUSIONS AND FUTURE WORKS

This paper presented a detailed methodology to effectively design a lateral control algorithm for a two-steering-axle off-road vehicle. A bicycle model was proposed in Section 2 that explicitly takes into account the soil slopes. On this basis, a feedforward and feedback architecture was considered, and sequentially synthesized. Uncertainties were explicitly taken into account during control synthesis. Large uncertainties ranges of the key parameters of the vehicle's model were considered, and trade-offs between performance and robustness were finely optimized in a systematic way. This approach involved a multi-model and multi-objective H_2/H_∞ control problem. Simulation based on a detailed model and realistic scenarios was performed; the results were considered very promising according to the simulation experts of the company Secom Engineering.

The industrial applications addressed here are quite wide for several reasons. First, the control architecture is simple enough to be implemented on a large variety of embedded computers. The memory allocation and the number of operations are negligible compared to other solutions. Second, the

H_2 / H_∞ control synthesis provides nice robustness properties and can easily adapt to various kinds of two-steering-axle off-road vehicles. Forthcoming works will focus on a modular integration of the longitudinal and lateral controls with anti-skid and roll stability control devices. The online estimation of certain poorly known and possibly variable parameters will be considered with a view to enable potential online adaptation of the control for the case of higher speeds applied to agricultural vehicles in particular.

REFERENCES

Apkarian, P., Gahinet, P., and Buhr, C. (2014). Multi-model, multi-objective tuning of fixed-structure controllers. *2014 European Control Conference*, 42, 856–861.

Arcak, M. and Kokotović, P. (2001). Feasibility conditions for circle criterion designs. *Systems & Control Letters*, 42(5), 405–412.

Attia, R., Orjuela, R., and Basset, M. (2012). Coupled longitudinal and lateral control strategy improving lateral stability for autonomous vehicle. In *2012 American Control Conference (ACC)*, 6509–6514. IEEE.

Bakker, E., Nyborg, L., and Pacejka, H.B. (1987). Tyre modelling for use in vehicle dynamics studies. In *SAE International Congress and Exposition*.

Bury, G., Zajdel, R., and Sośnica, K. (2019). Accounting for perturbing forces acting on galileo using a box-wing model. *Springer*, 23(3), 74.

Chevrel, P. (2013). Methodology of the State Approach Control. In P. de Larminat (ed.), *Analysis and Control of Linear Systems*, Wiley-ISTE, 55. Wiley-ISTE.

De Larminat, P. (2007). *Automatique appliquee*. Hermes Science: Lavoisier.

Deremetz, M. (2018). Contribution à la modélisation et à la commande de robots mobiles autonomes et adaptables en milieux naturels. PhD thesis.

Deremetz, M., Lenain, R., Couvent, A., Cariou, C., and Thuilot, B. (2017). Path tracking of a four-wheel steering mobile robot: A robust off-road parallel steering strategy. In *2017 European Conference on Mobile Robots (ECMR)*, 1–7.

Fernandez, B., Herrera, P.J., and Cerrada, J.A. (2019). A simplified optimal path following controller for an agricultural skid-steering robot. *IEEE Access*, 7, 95932–95940.

Fnadi, M., Plumet, F., and Benamar, F. (2019). Model predictive control based dynamic path tracking of a four-wheel steering mobile robot. In *2019 IEEE/RSJ International Conference on Intelligent Robots and Systems (IROS)*, 4518–4523. IEEE.

Hirschberg, W., Rill, G., and Weinfurter, H. (2003). User-appropriate tyre-modelling for vehicle dynamics in standard and limit situations. *Vehicle System Dynamics*, 38(2), 103–125.

Huang, X., Zhang, H., Zhang, G., and Wang, J. (2014). Robust weighted gain-scheduling h_∞ vehicle lateral motion control with considerations of steering system backlash-type hysteresis. *IEEE Transactions on Control Systems Technology*, 22(5), 1740–1753.

Jazar, R.N. (2009). *Vehicle dynamics: theory and applications*. Springer, corrected at 3. printing edition.

Kwakernaak, H. and Sivan, R. (1969). *Linear optimal control systems*, volume 1072. Wiley.

Lenain, R., Thuilot, B., Cariou, C., and Martinet, P. (2009). Multi-model based sideslip angle observer: Accurate control of high-speed mobile robots in off-road conditions. In *2009 IEEE/RSJ International Conference on Intelligent Robots and Systems*, 1197–1202. IEEE.

Markets and Markets (2020). *Agricultural Robots Market with COVID-19 Impact Analysis*. Available at https://www.marketsandmarkets.com/Market-Reports/agricultural-robot-market-173601759.html, (access date: May 7, 2021).

Mourad, L., Claveau, F., and Chevrel, P. (2014). Direct and steering tilt robust control of narrow vehicles. *IEEE Transactions on Intelligent Transportation Systems*, 15(3), 1206–1215.

Mustaki, S., Chevrel, P., Yagoubi, M., and Fauvel, F. (2018). Efficient multi-objective and multi-scenarios control synthesis methodology for designing a car lane centering assistance system. In *2018 European Control Conference (ECC)*, 929–934. IEEE.

Mustaki, S., Nguyen, A.T., Chevrel, P., Yagoubi, M., and Fauvel, F. (2019). Comparison of two robust static output feedback h2 design approaches for car lateral control. In *2019 18th European Control Conference (ECC)*, 716–723. IEEE.

Mustaki, S.E. (2019). Outils de pré-calibration numérique des lois de commande de systèmes de systèmes: application aux aides à la conduite et au véhicule autonome. PhD thesis.

Rajamani, R. (2012). *Vehicle dynamics and control*. Mechanical engineering series. Springer, 2. ed edition.

Rill, G. (2013). Tmeasy : A handling tire model based on a three-dimensional slip approach. In *XXIII International Symposium on Dynamic of Vehicles on Roads and on Tracks (IAVSD)*.

Sadabadi, M.S. and Peaucelle, D. (2016). From static output feedback to structured robust static output feedback: A survey. *Annual Reviews in Control*, 42, 11–26.

Shuai, Z., Zhang, H., Wang, J., Li, J., and Ouyang, M. (2014). Lateral motion control for four-wheel-independent-drive electric vehicles using optimal torque allocation and dynamic message priority scheduling. *Control Engineering Practice*, 24, 55–66.

Walter, P.G. and Noll, D. (2015). Optimization-based control design techniques and tools. *Encyclopedia of Systems and Control*.

Zames, G. (1996). Input-output feedback stability and robustness. *IEEE Control Systems Magazine*, 16(3), 61–66.